2020

Multi-temporal scale analysis of complementarity between hydro and solar power along an alpine transect

T. Pérez Ciria

H. D. Puspitarini

G. Chiogna

B. François

M. Borga

Science of the Total Environment 741 (2020) 140179

Contents lists available at ScienceDirect

Science of the Total Environment

journal homepage: www.elsevier.com/locate/scitotenv

Multi-temporal scale analysis of complementarity between hydro and solar power along an alpine transect

T. Pérez Ciria [a,*], H.D. Puspitarini [b], G. Chiogna [a,c], B. François [d], M. Borga [b]

[a] Institute of Geography, University of Innsbruck, Innrain 52f, 6020 Innsbruck, Austria
[b] University of Padova, Dept. Land, Environment, Agriculture and Forestry, Padova, Italy
[c] Faculty of Civil, Geo and Environmental Engineering, Technical University of Munich, Arcistr. 21, 80333 Munich, Germany
[d] Department of Civil and Environmental Engineering, University of Massachusetts Amherst, Amherst, MA 01003, USA

HIGHLIGHTS

- Definition of wavelet-based complementarity index (WBCI) at multiple temporal scales
- WBCI quantifies the scale-dependent complementarity among variable renewable energies
- Detection of relevant periodicities of renewable energies and electricity demand
- Assessment of the energy balance for different energy mix combinations
- Wavelet analyses offer a robust framework for practical renewable energy balance studies

GRAPHICAL ABSTRACT

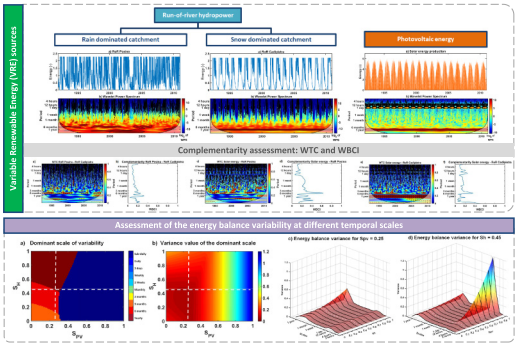

ARTICLE INFO

Article history:
Received 12 May 2020
Received in revised form 10 June 2020
Accepted 10 June 2020
Available online 15 June 2020

Editor: Fernando A.L. Pacheco

Keywords:
Run-of-the river hydropower
Solar power
Energy complementarity
Wavelet analysis
Alpine transect

ABSTRACT

Variable renewable energy sources display different space-time variability driving the availability of energy generated from these sources. Complementarity among variable renewable energies in time and space allows reducing the variability of power supply and helps matching the electricity demand curve. This work investigates the temporal structure of complementarity along an alpine transect in North-East Italy, considering a 100% renewable energy mix scenario composed by photovoltaic and run-of-the-river energy. We analyze the dominant scales of variability of variable renewable energy sources and electricity demand. In addition, we introduce a new metric, the wavelet-based complementarity index, to quantify the potential complementarity between two different energy sources. We show that this index varies at different temporal scales and it helps explaining the discrepancy between demand and supply in the study area. Continuous and discrete wavelet analyses are applied to assess the energy balance variability at multiple temporal scales and to identify the optimal mix of renewable energies, respectively. This work describes therefore an effective approach to investigate the temporal-scale dependency of the variance in the energy balance and can be further extended to different and more complex situations.

Abbreviations: ARPAV, regional environmental protection agency of Veneto; COI, cone of influence; CWT, continuous wavelet transform; DWT, discrete wavelet transform; GWS, global wavelet spectrum; ICHYMOD, integrated catchment hydrological model; PV, photovoltaic; RoR, run-of-river; S_H, sharing coefficient of run-of-river hydropower between hydroclimatic regions; S_{PV}, sharing coefficient of solar power; VRE, variable renewable energy; WBCI, wavelet-based complementarity index; WPS, wavelet power spectrum; WT, wavelet transform; WTC, wavelet transform coherence.

* Corresponding author.
E-mail address: teresa.perez-ciria@uibk.ac.at (T. Pérez Ciria).

https://doi.org/10.1016/j.scitotenv.2020.140179

1. Introduction

Variable Renewable Energy (VRE) sources, such as solar, hydro and wind power, are paramount for the success of the energy transition (Jacobson and Delucchi, 2011; IEA, 2018). The availability of VRE generation follows from the spatial and temporal variability of their hydrometeorological forcing that include, among others, solar radiation, wind velocity, air temperature, precipitation and river runoff (Troccoli et al., 2014; François et al., 2014; Widén et al., 2015; Engeland et al., 2017; Wörman et al., 2017). Although the electricity demand varies across seasonal, weekly, and sub-daily time scales, its variability is significantly lower than the one stemming from each VRE taken individually (Engeland et al., 2017; Staffell and Pfenninger, 2018). As a result, large integration of VRE into the electricity system will often lead to periods during which generation is either significantly larger or lower than the electricity demand. The former situation might lead to curtailment of VRE production means, while the latter requires additional generation to supply the residual load.

Several strategies are commonly used to ensure the balance between electricity generation and demand. They include transport through the electricity grid networks (Weitemeyer et al., 2015; François et al., 2017b; Brown et al., 2018; Chowdhury et al., 2020), demand-side management (Roldán Fernández et al., 2016; Kies et al., 2016), optimization of the schedulable production means (Ming et al., 2018), use of storage (Heide et al., 2010; Weitemeyer et al., 2016; Clerjon and Perdu, 2019), and use of the complementarity among VRE sources (François et al., 2016a, 2016b; Kougias et al., 2016). The concept of complementarity translates the fact that, by combining several VREs both in space and time, the variability of the aggregated generation becomes lower than the one stemming from any individual source, which significantly increases the system capability of satisfying electricity demand (Han et al., 2019; Jurasz et al., 2020). Temporal complementarity depends primarily on the co-variability between renewable energy sources for two main reasons. First, energy sources must vary within the same order of magnitude to be efficiently combined and satisfy the energy load (François et al., 2016a, 2016b). Secondly, complementarity depends on the correlation among the VREs. A strongly negative correlation between two VRE sources highlights large potential for complementarity; the correlation however often depends on the temporal scale (Widen, 2011; François et al., 2016a). Another often-used metric to assess complementarity between VREs and electricity demand is the variability of the deviations between generation and demand; the so-called 'energy balance'. The complementarity is high when the variability of the energy balance is low (Jurasz et al., 2020; Kougias et al., 2016; Puspitarini et al., 2020). Other complementary indexes exist, although applications beyond their authors' work are sparse (Borba and Brito, 2017; Beluco et al., 2019; Canales et al., 2020).

The abovementioned studies highlight that the multiscale variability stemming from the VRE sources, ranging from local to meso- and synoptic-scales and from seconds to decades, leads to various degrees of complementarity depending on the considered temporal scale (Engeland et al., 2017). The temporal scales considered as relevant in these works required an a priori selection for the specific system, which does not necessarily align with the patterns of variability of the energy sources. Moreover, the dominant scales of variability of the VRE sources and electricity demand might significantly vary depending on the study region. An analysis that explicitly permits to identify the most significant scales of variability for the considered system and to assess temporal complementarity at those specific scales is still missing, to the best of our knowledge. Moreover, a complementarity metric which helps to identify the potential complementarity between VRE sources across the continuous range of temporal scales is lacking in the literature. In this study, we aim at filling this gap by applying Wavelet analysis (WA). WA represents a robust methodology for providing multiresolution representation of geophysical and socioeconomic time series (Alam et al., 2014; Bonkaney et al., 2019; Chang et al., 2017). Representation of the time series data into time domains makes possible to extract useful information about temporal cyclic events existing in the underlying signal.

The main contribution of our work is to apply wavelet analysis for: i) the identification of the dominant scales of variability of the VRE sources and electricity demand, which has proved to be an indispensable step to cope with the uncertainty associated to an a priori selection of the temporal scales; ii) the introduction of a new temporal complementarity metric, termed wavelet-based complementarity index – WBCI, to identify the potential complementarity among VRE sources across the continuous range of temporal scales; iii) the detection of the dominant periodicities that arise from the energy balance assessment of the different energy mix combinations; iv) the quantitative evaluation of the variance of the energy balance at multiple temporal scales. Based on the wavelet analyses, we obtain a complete picture of the performance of the different energy mix combinations while we are able to focus on the previously detected dominant temporal scales. We focus in this work on the complementarity between Run-of-River (RoR) hydropower and solar photovoltaic (PV) power.

2. Methodology

2.1. Energy mix and balance under 100% renewable scenario

The electric energy balance is examined on the basis of two main assumptions. The first assumption concerns the well-known '100% renewable' scenario, which translates into a hypothetic configuration where power generation from solar PV and RoR hydropower equals the electricity demand on average over the considered study period. This scenario is commonly used for assessing the complementarity among several energy sources (von Bremen, 2010; Heide et al., 2010; Raynaud et al., 2018; François et al., 2018). We also assume no power transmission limitation or loss within the study region. This configuration ensures the overall energy balance is null over the analyzed period (i.e., the difference between total generation and total electricity demand). However, temporal variations of both generation and consumption lead to mismatches that we analyze as indicator of the complementarity among energy sources. The models used to simulate electricity production from RoR and PV, and electricity demand are described in the Supplementary material.

In the scenario of 100% renewable mix, electricity generation from RoR and solar PV are scaled to ensure equality between average generation and demand over the considered period as follows:

$$p(t) = \frac{P(t)}{\langle P(t) \rangle} \tag{1}$$

where $p(t)$ is the scaled electricity generation (either from solar PV or from RoR), $P(t)$ is the actual electricity generation, and $\langle\rangle$ is the average operator over the considered time period.

P_{RoR} is calculated as follows with a mixture of snow- and rain-dominated runoff regimes:

$$P_{RoR}(t) = S_H \cdot P_{RoR_{Snow}}(t) + (1 - S_H) \cdot P_{RoR_{Rain}}(t) \tag{2}$$

where $P_{RoR_{Snow}}$ and $P_{RoR_{Rain}}$ are *RoR* power generation from snowmelt and rainfall dominated runoff regimes and S_H is the sharing coefficient between the two hydro-climatic regions ($0 \le S_H \le 1$). When $S_H = 1$, the RoR production is only from the snowmelt dominated regime and when $S_H = 0$, the RoR production is only from the rainfall dominated regime.

RoR and *PV* mixed power generation scenarios are obtained by combining *PV* and *RoR* power generation using a sharing coefficient denoted

S_{PV}. Power generation from a combination of solar PV and RoR is then obtained as follows:

$$p_{mix} = s_{PV}p_{PV} + (1-s_{PV})p_{RoR} \quad (3)$$

where p_{mix} is power generation from the combined system, S_{PV} is the sharing coefficient of solar power, p_{PV} is scaled solar power generation, p_{RoR} is scaled hydropower generation.

2.2. Wavelet analysis

Wavelet Transform (WT) is a powerful tool to determine the relevant scales of variability of a signal and identify changes in the modes of variability within non-stationary time series (Grinsted et al., 2004; Torrence and Compo, 1998). Wavelet analysis is a widely used time series analysis technique due to its versatile applicability, especially for hydro-climatic time series analysis (Carey et al., 2013; Guan et al., 2011; Labat, 2010; Labat et al., 2000; Labat et al., 2004; Marcolini et al., 2017; Nalley et al., 2012; Pérez Ciria and Chiogna, 2020; Rathinasamy et al., 2014). More recently, it was applied in the energy sector (Bonkaney et al., 2019), focusing for example on the integration between solar and wind power (Alam et al., 2014; Chang et al., 2017), and to analyze the effects of hydropower production on the environment (Chiogna et al., 2018; Pérez Ciria et al., 2019; Zolezzi et al., 2009). In the present section we have included a brief description of continuous wavelet transform (CWT), wavelet transform coherence (WTC), the suggested new complementarity metric (wavelet-based complementarity index-WBCI), and discrete wavelet transform (DWT) and their application in our study. In the Supplementary material we provide a more mathematical description and we refer the reader to Torrence and Compo (1998) and Grinsted et al. (2004) for more details.

2.2.1. Continuous wavelet transform (CWT)

We apply continuous wavelet transform (CWT) to show how electricity demand and energy production might behave differently depending on the considered temporal scale. We compute also the CWT of the energy balance to assess the suitability of different VRE combinations. CWT analysis is performed by computing the convolution of the time series with a scaled and translated version of a mother wavelet. In our case, we select the widely applied Morlet mother wavelet (Fu et al., 2012; Nalley et al., 2016; Chang et al., 2017), since it provides a good compromise between the time and frequency resolution (Grinsted et al., 2004; Labat, 2006; Schaefli et al., 2007).

2.2.2. Wavelet transform coherence (WTC)

Based on the CWT, it is possible to compute the wavelet transform coherence (WTC) between two time series, i.e., the local correlation between two CWTs. In fact, the value of the WTC can be interpreted as the squared correlation coefficient of the time series components. The WTC analysis also allows us to identify if two signals are in phase or in counter phase and when a change in the phase may occur (Torrence and Webster, 1999). This is represented in the WTC figures using an arrow that points to the right when two signals are in phase (i.e., the phase shift α between the two signals is 0) and gradually turns to the left the larger is the phase difference between the two signals. When two signals have a phase shift $\alpha = \pi/2$ the arrow points to the bottom, when the phase sift $\alpha = \pi$ the arrow points to the left. The 95% significance level and the confidence intervals of all CWT and WTC are calculated against red noise background using Monte Carlo methods.

2.2.3. Wavelet-based complementarity index (WBCI)

Based on the WTC, we introduce the wavelet-based complementarity index (WBCI) as new metric to assess the complementarity between energy sources at multiple temporal scales. The index incorporates information about the time lag between the investigated variables and it ranges from 0 to 1. The WBCI is computed for every temporal scale s as follows:

$$WBCI_s = \frac{1}{N}\sum_{i=1}^{N} C_{i,s} * \left(\frac{1-\cos(\alpha_{i,s})}{2}\right) \quad (4)$$

where C represents the coherence value between the two signals for a specific scale s and a specific time i, α is the phase angle that represents the time lag between the investigated variables and N is the length of the time series.

Two variables that present very high coherence ($C_{i,s} \approx 1$ for all $i = 1, \ldots N$) at a specific temporal scale s and are consistently in phase ($\alpha_{i,s} \approx 0$ for all $i = 1, \ldots N$) will still have very low (close to 0) WBCI values, indicating low complementarity between the variables at this specific temporal scale. On the contrary, high coherence values at a specific temporal scale, which are consistently in counter-phase ($\alpha_{i,s} \approx \pi$ for all $i = 1, \ldots N$), will have very high (close to 1) WBCI values, indicating very high complementarity between these variables at this temporal scale. When no coherence is detected between the variables, the WBCI values are also close to 0. If the coherence is equal to one, WBCI ≈ 0.5 for $\alpha_{i,s} \approx \frac{\pi}{2}$ or $3\pi/2$ (quarter-cycle phase lag for all $i = 1, \ldots N$). The corresponding lag in time depends on the duration of the cycle and therefore the scale s. Thus, WTC and WBCI are computed to compare the different energy sources time series among them as a measure of their potential complementarity.

We applied the WTC and computed the associated WBCI (Fig. 1) to three combinations of synthetic signals (data1 with data2, data3, and data4), defined in Eqs. (5) - (8), where ε is Gaussian noise with 0 mean and standard deviation equal to 1 and t is the time in hours.

$$data1 = \sin\left(\frac{2\pi t}{24}\right)/2 + \sin\left(\frac{2\pi t}{365*24}\right) + \cos\left(\frac{2\pi t}{2*365*24}\right) + \varepsilon \quad (5)$$

$$data2 = \sin\left(\frac{2\pi t}{24} + \pi\right)/2 + \sin\left(\frac{2\pi t}{365*24}\right) + \varepsilon \quad (6)$$

$$data3 = \sin\left(\frac{2\pi t}{24} + \pi\right)/2 + \sin\left(\frac{2\pi t}{365*24} + \frac{\pi}{2}\right) + \varepsilon \quad (7)$$

$$data4 = \sin\left(\frac{2\pi t}{24} + \pi\right)/2 + \sin\left(\frac{2\pi t}{365*24} + \pi\right) + \varepsilon \quad (8)$$

The first synthetic signal is characterized by a daily, a yearly, and a 2 years periodicity. Random noise is included to obtain a signal resemblance to the target time series and to guarantee the significance of the analysis. The same daily periodicity ($\sin(\frac{2\pi t}{24} + \pi)/2$) is considered for data2, data3 and data4, which maintains the same amplitude from the daily periodicity of data1, but with a time shift of π (counter-phase signals). Focusing on the yearly scale, both data1 and data2 share the same periodicity (signals in phase). Data3 in relation to data1 presents a π/2 time shift at the yearly scale. Data4 presents a π time shift in relation to data1 for the yearly scale (counter phase signals). Fig. 1a shows the synthetic time series for the time period from 1992 to 2012 (selected for illustrative purposes) and Fig. 1b displays the daily cycle of the signals.

The WTC of the abovementioned combinations is shown in Fig. 1c (data1 and data2), Fig. 1e (data1 and data3), and Fig. 1g (data1 and data4). Focusing on the daily scale we can observe high wavelet coherence values and arrows pointing to the left (representing a π shift of the analyzed signals) for the three different combinations. The WBCI in Fig. 1d, f and h presents a very high value (>0.9) for the daily scale, since they are counter-phase signals for the whole represented time span (Fig. 1b). At the yearly scale we defined three different situations. First, the WTC in Fig. 1c illustrates that data1 and data2 are highly coherent and in phase (arrows pointing to the right). The suggested WBCI is computed such that it drops to 0 when two signals are completely in

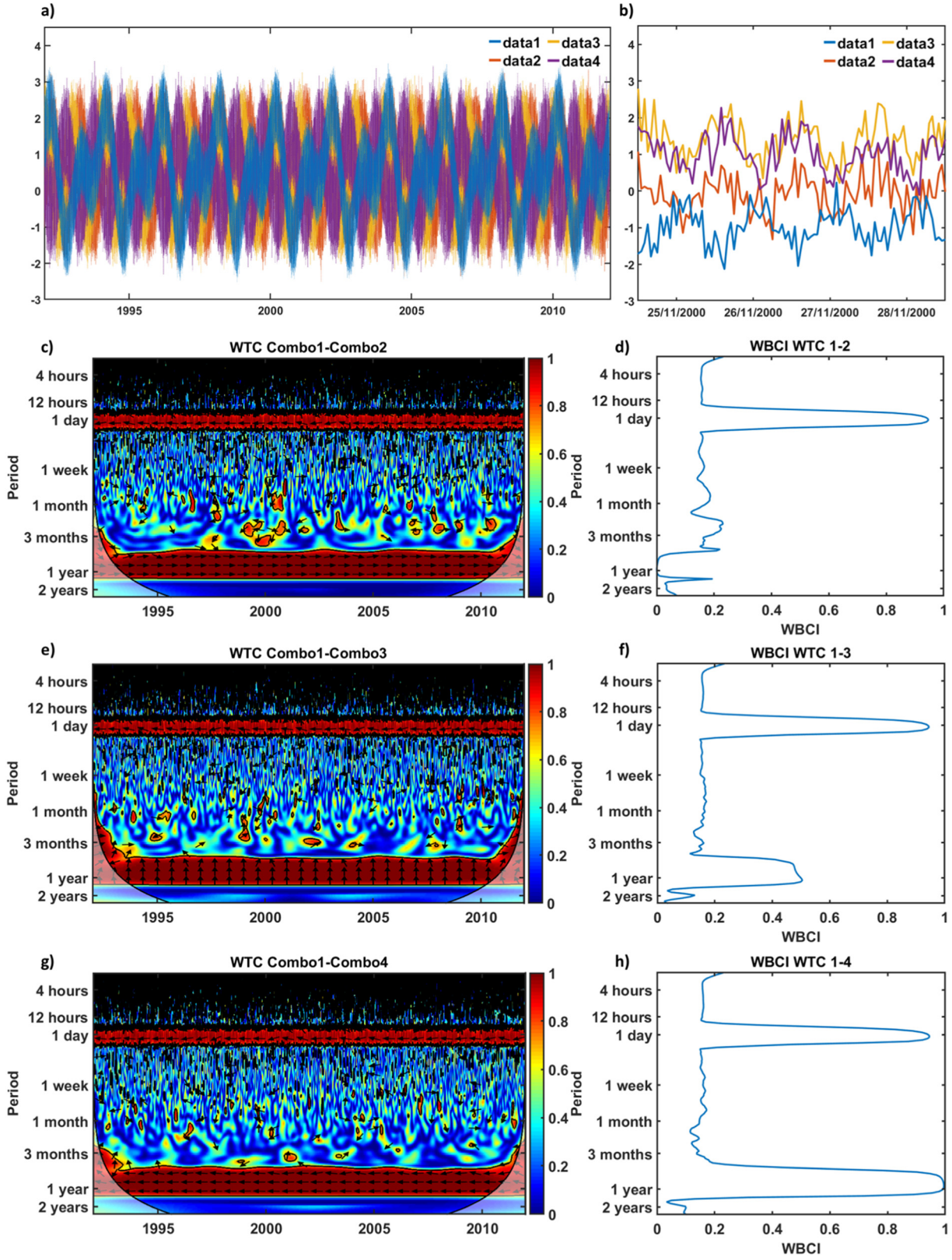

Fig. 1. Wavelet Transform Coherence (WTC) and wavelet-based complementarity index (WBCI) of synthetic signals. Plot a) shows the synthetic time series for the time period from 1992 to 2012. Plot b) zooms in plot a) and shows the daily cycle of the synthetic signals. The WTC of the three different combinations is shown in plot c) (data1 and data2), plot e) (data1 and data3), and plot g) (data1 and data4). Blue color means no coherence between the variables (value equal to 0) and red color means total coherence (value equal to 1). Arrows show the relative angular phase relationships between the signals. Right pointing arrows depict in-phase, while left pointing arrows represent anti-phase relationship. Vertically upward arrows depict a lead of π/2 or one-quarter (downward a lag) between signals. Next to each WTC the values of the associated WBCI are shown (right plots): plot d) data1 and data2, plot f) data1 and data3, and plot h) data1 and data4.

phase during the whole analyzed time span. This is the case of data1 and data2 at the yearly scale, as we can observe in Fig. 1d. At the yearly scale, the WTC of the second combination (data 1 and data3) shown in Fig. 1e illustrates two signals with high coherence values, but out of phase. In this case, the arrows are pointing up and represent a π/2 time shift. Fig. 1f displays a higher value of WBCI (WBCI = 0.5) at the yearly scale in comparison with the first combination in Fig. 1d (WBCI = 0). Finally, Fig. 1g shows the WTC between data1 and data4. We can observe that at the yearly scale high coherence values are present (as they were in Fig. 1c and e), but in this plot the arrows are pointing left, which means that the signals are in counter-phase (π time shift). In the context of complementarity, this third situation represents the optimal combination of two different VRE sources and it is captured by the suggested WBCI (Fig. 1h), where the WBCI = 1 at the yearly scale. As final remark, we would like to highlight that the use of synthetic signals allows us to verify the validity of the suggested complementarity metric and shows a threshold of significance in WBCI = 0.15 (values observed for non-dominant scales due to Gaussian noise). However, in comparison with the analysis of synthetic signals the magnitude of the WBCI is expected to be lower for the analysis of VRE sources, since the energy production is determined by geophysical variables (e.g.: solar radiation, temperature, and streamflow), which are characterized by a more complex behavior than the synthetic time series given by Eqs. (5)–(8).

2.2.4. Discrete wavelet transform (DWT)

It is not possible to reconstruct the original signal from the coefficients derived from the continuous wavelet transform (CWT) analysis. Consequently to study how the variance of the signal is distributed among different temporal scales we apply the discrete wavelet transform (DWT). In this case, we decouple the signal into progressively finer octave bands. This means that DWT, unlike CWT, uses algorithms that operate on scales with discrete numbers normally based on integer powers of two (Nalley et al., 2012; Maheswaran and Khosa, 2012; Tiwari and Adamowski, 2013). The DWT analysis enables us to detect patterns that are not visible in the raw data and is implemented to detect changes in the time series variance. In our study, we use DWT to: i) quantitatively evaluate the variability of the energy balance computed for the different energy mix combinations at multiple temporal scales; and ii) map variance changes focusing on the dominant scales previously identified using CWT. The lowest variance values of the energy balance determine the optimal energy mix for the region of study. The DWT is hence used to quantitatively evaluate the energy balance variability at multiple temporal scales and assist us in the selection of the optimal energy mix.

3. Study area

To analyze the complementarity among VREs, we consider two case studies located on the opposite edges of a climate transect connecting the Alpine crest to the Veneto plain in North-Eastern Italy. This transect provides a range of climatic variability and includes runoff regimes that gradually vary from snow-melt dominated to rainfall dominated, with a ratio of solid to total precipitation decreasing from 0.6 in the northern part to almost 0 in the Veneto plain. In addition, this region is characterized by a relatively high level of small RoR hydropower stations related to the initiatives of private actors or small communities, while the rate of PV equipment is rather high thanks both to public subsidies and easiness of installation (Moser et al., 2014; GSE, 2019).

We focus specifically on two catchments located in the transect (Fig. 2), which are of similar size and characterized by different hydroclimatic regimes, Aurino at Cadipietra (149.8 km^2) and Posina at Stancari (116 km^2). The altitude range of Aurino at Cadipietra is from 1049 to 3263 m a.s.l. and for Posina at Stancari is from 390 to 2146 m a.s.l. Aurino at Cadipietra has a snow-dominated regime with a mean annual precipitation around 1500 mm and a fraction of precipitation as snow around 60%. The mean annual streamflow is 6.2 m^3/s and the peak flow occurs usually in summer due to snow and ice-melt contribution. As a rain-dominated catchment, Posina at Stancari is characterized by a fraction of precipitation as snow around 20%. The mean annual precipitation and streamflow for this basin is 1325 mm and 3.7 m^3/s. In Posina at Stancari, streamflow presents two peaks, in spring and autumn, with >70% of the mean annual precipitation during these seasons.

The period selected for the analysis spans from 1992 to 2012. Over this period, solar radiation and temperature data are available from 17 stations managed by the Regional Environmental Protection Agency of Veneto (ARPAV) to simulate solar PV generation and electricity demand. Since the measured time series at the gauging stations of Aurino at Cadipietra and Posina at Stancari present some data gaps that make the wavelet analysis difficult to interpret, we based the analysis on hourly simulated runoff. From the different rainfall-runoff models (Moore, 2007; Balbastre-Soldevila et al., 2019; García-Bartual and Andrés-Doménech, 2017; Kratzert et al., 2018), we applied the Integrated Catchment Hydrological Model (ICHYMOD) (Norbiato et al., 2009; François et al., 2017a). For more detailed information about ICHYMOD the authors refer to Puspitarini et al. (2020) and Zaramella et al. (2019).

4. Results

4.1. Wavelet analysis of electricity demand and energy production

4.1.1. Continuous wavelet transform and global wavelet spectrum

CWT provides us a clear understanding of the scales of variability that characterize each of the considered variables (scaled values): electricity demand (Fig. 3), energy production of RoR located in the rain dominated catchment Posina (Fig. 4), energy production of RoR located in the snowmelt dominated catchment Cadipietra (Fig. 5), and solar energy production (Fig. 6). The upper panel of the figures (panel a) in Figs. 3–6) shows the time series values from January 1992 through December 2012; plot b) shows the hourly data displaying a typical daily and weekly cycle of each considered variable and in Figs. 4–6 the electricity demand (hourly data) is included for comparison purposes and is especially relevant to interpret the energy balance assessment included in our work. The CWT power spectrum is shown for the different variables in Figs. 3–6 plot c. The global power spectrum (i.e., the time averaged wavelet spectrum) is located on the right side of the CWT power spectrum (Figs. 3–6 plot d). The global wavelet spectrum (GWS) reveals the relevant scales as the ones with wavelet power larger than a 95% significance level developed from a red-noise background process (black dashed line).

In Fig. 3, the CWT of the electricity demand time series shows that this signal is characterized by specific scales of variability (12 h, 1 day, 3 days, 1 week, 3–6 months and 1 year), which are rather stationary throughout the period 1992–2012. Some scales are based on geophysical forcing (1 day, seasonal, 6 months, 1 year) while others follow our social dynamic (i.e., weekdays – weekend). An optimal combination of VRE production should be able to resemble this signal. However, we can observe that for the case study considered in this work, none of the available renewable resources is characterized by the same scales of variability as electricity demand (Figs. 3–6).

Considering the scales of variability, the behavior of RoR hydropower production from rain fed catchments such as Posina (Fig. 4) displays as major periodicity associated to the 6 months scale. The signal is strongly controlled by the effects of meteorological rainfall events that lead to flood events and a rapid recession. RoR generation at Posina is characterized by two peaks that occur usually in April and between October and December. Interestingly, the 6-months pattern associated to these peaks does not appear with the same intensity every year in the power spectrum. This could be due to the low-frequency variability that influences the precipitation falling during the raining season with a large deviation between interquartile from October through

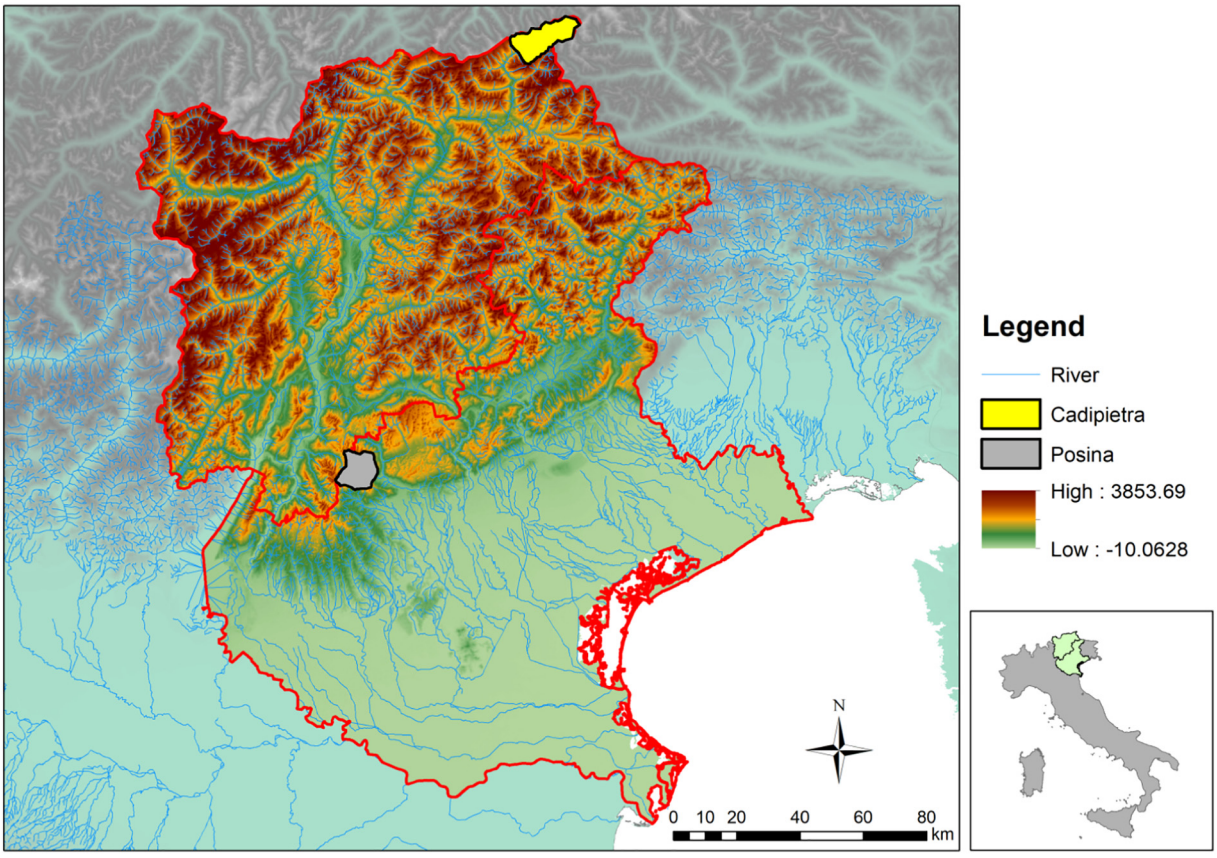

Fig. 2. The study transect with the location of the two river basins: Aurino at Cadipietra and Posina at Stancari.

December (François et al., 2018). The 6 months scale periodicity can be also noticed in the global wavelet spectrum (GWS) reaching a higher wavelet power value than the yearly scale.

RoR hydropower production from snow-melt dominated catchment, such as Cadipietra (Fig. 5) is characterized by a strong seasonality, due to the influence of the snowpack dynamic on streamflow

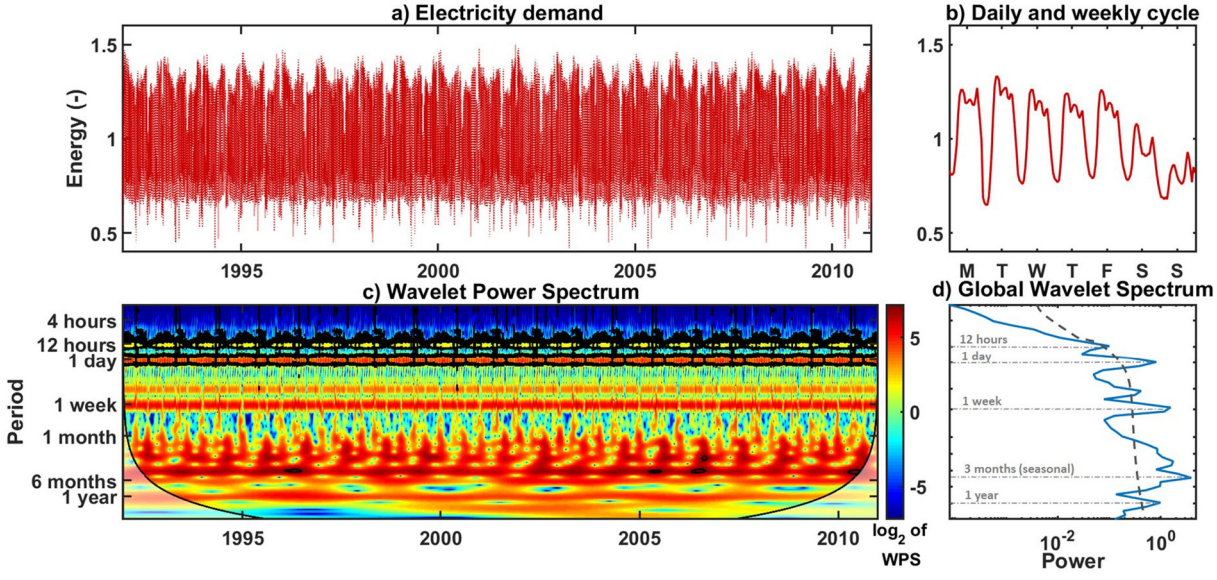

Fig. 3. Time series (plot a), daily and weekly cycle (plot b), CWT power spectrum (plot c), and global wavelet spectrum (plot d) of electricity demand (scaled values). Plot b shows the daily and weekly cycle of the electricity demand (hourly data) (7.05.2001–14.05.2001). The CWT spectrum shows time (years) on the ordered axis, and the analyzed scales (period) on the abscissa. Red colors represent high wavelet power values (i.e., strong periodicity), blue colors represent low values of the wavelet power (i.e. weak periodicity). Areas circled with a black contour represent 5% statistically significant results. The cone of influence (COI), region of the wavelet spectrum where edge effects might be important, it is shown as a white shaded area. The global wavelet spectrum (GWS) highlights the relevant scales of variability. The dashed black line depicts the 95% significance level against red-noise background spectra.

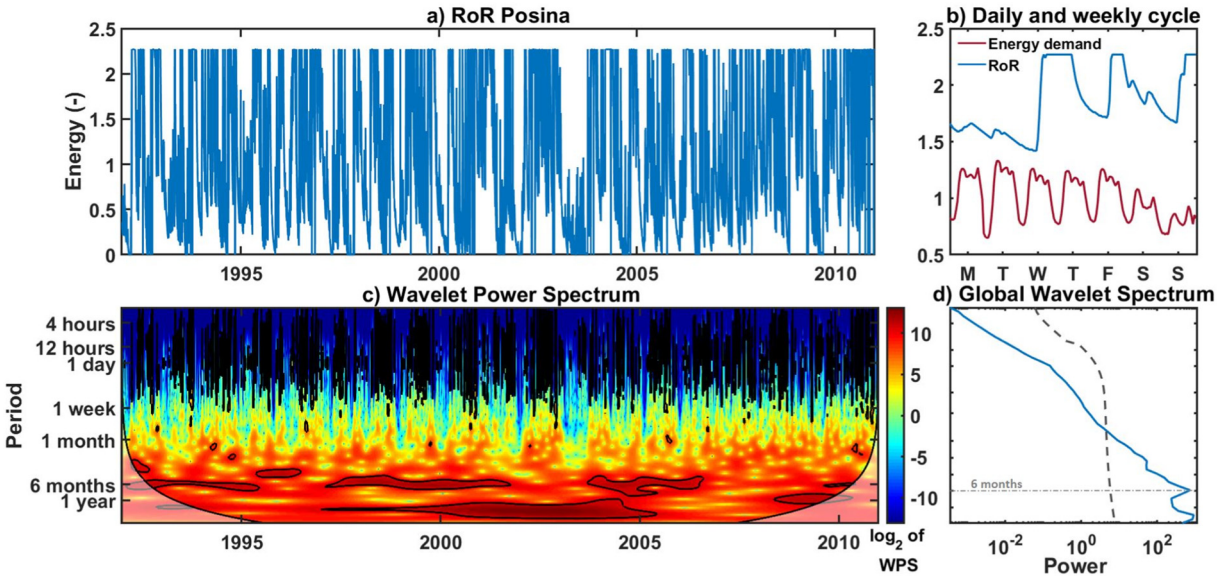

Fig. 4. Time series (plot a), daily and weekly cycle (plot b) (7.05.2001-14.05.2001), CWT power spectrum (plot c), and global wavelet spectrum (plot d) of energy production (scaled values) of RoR located in Posina (rain dominated catchment). In plot b) the demand time series is included for magnitude comparison. The explanation of the figure is analogous to the one given in Fig. 3.

variability. In the spring and early summer months, we can observe the occurrence of a strong component at the sub-daily scale, typical for snow melting processes. In Fig. 5b) the daily cycle is easily recognizable for the RoR energy production in spring, while a constant production is present for winter months, and a more fluctuating energy production dependent on rainfall events is associated to late summer, due to the increasing importance of liquid precipitation. Fig. 5c) displays that the seasonal variability resulting from the snowpack accumulation and melt dynamic above-described, is the dominant scale of variability. In Fig. 5d) the Global Wavelet Spectrum (GWS) shows the peak at the yearly scale, and additionally a peak associated to the daily periodicity. This daily peak is, however, not statistically significant (it does not exceed the black dashed line) due to the fact that is not present during the whole year, but only during the specific months when melting processes become relevant. In contrast to Posina, the 6 months scale of variability is not present for Cadipietra, which becomes an additional incentive for combining the two hydrological regimes.

Yearly periodicity is also highly important for solar radiation (Fig. 6c); this signal however is characterized by two additional relevant scales of variability at the daily and 12 h scales. Both of them are stronger during the summer months and decrease their wavelet power during winter time. Plot 5b is valuable to understand the magnitude of solar energy production (extreme behavior that ranges from null production at night to maximum values tripling and quadrupling electricity demand at midday) in comparison with RoR (more stable in general and practically constant during fall and winter months for the snow dominated catchments).

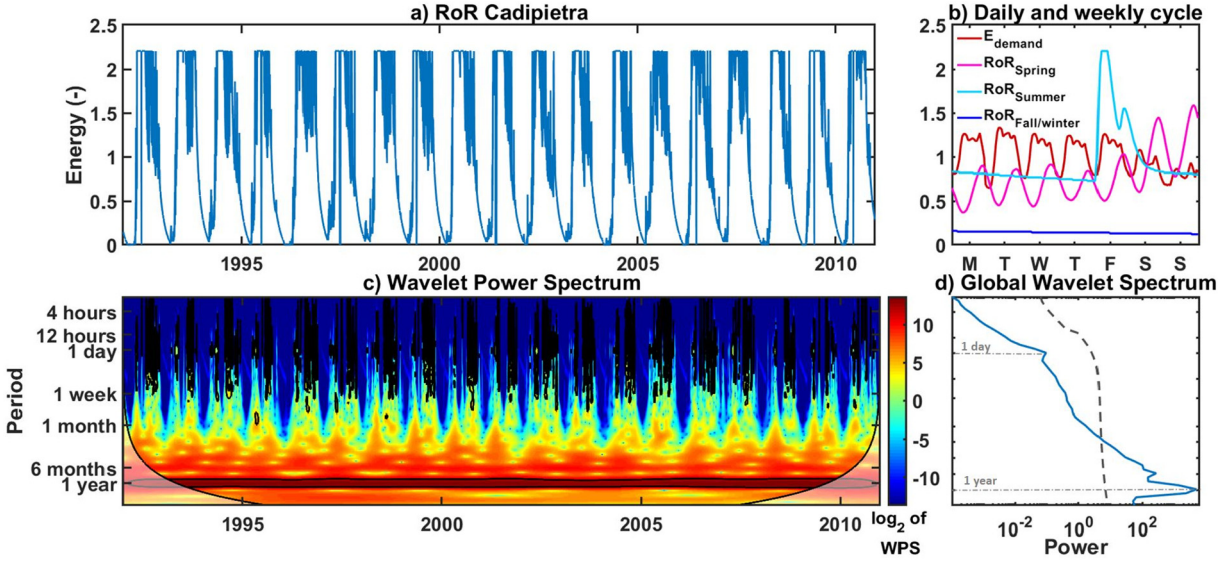

Fig. 5. Time series (plot a), daily and weekly cycle (plot b) (7.05.2001-14.05.2001 for demand and RoR spring, 10.09.2001-17.09.2001 for RoR summer and 08.01.2001-15.01.2001 for RoR winter representing the behavior also in fall), CWT power spectrum (plot c), and global wavelet spectrum (plot d) of energy production (scaled values) of RoR located in Cadipietra (snow dominated catchment). The explanation of the figure is analogous to the one given in Fig. 3.

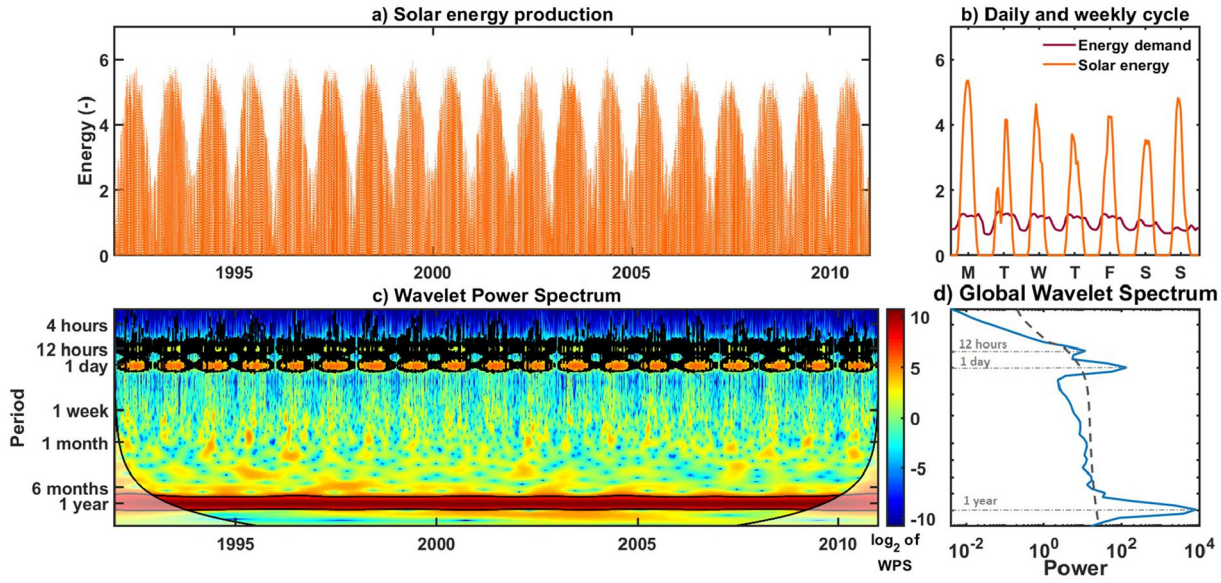

Fig. 6. Time series (plot a), daily and weekly cycle (plot b) (7.05.2001-14.05.2001), CWT power spectrum (plot c), and global wavelet spectrum (plot d) of solar PV energy production (scaled values). The explanation of the figure is analogous to the one given in Fig. 3.

The take-home message from the above wavelet analysis is threefold. First, the electricity demand highlights complex variability patterns embedded one with another. Second, none of the three considered VRE sources shows such complex patterns of variability. Third, the three considered VRE sources show significant differences in their mode of variability, which provides a strong incentive for mixing these energy sources.

4.1.2. Complementarity among energy sources using WTC

WTC analysis is applied to compare the CWT of two different energy sources as an indicator of their complementarity. In Fig. 7a we can observe that the coherence between energy production from RoR in Posina and RoR in Cadipietra is not stationary throughout the investigation period. In general, we can observe low coherence values. High coherence values are not present during the whole analyzed time span, but rather show an intermittent behavior. Focusing on the 6 months scale in the WTC of Fig. 7a, we observe (especially from 1992 till 2002, but also around 2005 and from 2008) high wavelet coherence values with arrows pointing down (π/2 phase shift), which represent a time lag between one and two months between runoff peaks. Notice that for Posina there is a runoff peak in April while for Cadipietra it usually takes place between May and June due to snow melting processes (implying between 1 and 2 months lag). In Fig. 7c the WTC between RoR from the rain dominated catchment and solar energy presents non-stationary coherence at the seasonal scale. The phase of the signals is variable (and often in counter phase). In contrast, in Fig. 7e we can observe that RoR from the snow dominated catchment has a strong stationary coherence with the solar energy signal at the yearly scale. Solar radiation intensity and temperature are the main triggers of melting processes, governing therefore not only the solar energy production, but the runoff yearly cycle of snow dominated catchments.

From the WBCI we can observe that focusing on short time scales WBCI values in Fig. 7b are nearly constant, while two peaks are present for the 12 h and daily scales in Fig. 7d and f. These WBCI values are slightly higher for the snow dominated catchment reaching 0.2 and 0.25 for the 12 h and daily scales, respectively (Fig. 7f), while WBCI = 0.17 in both peaks for RoR in Posina (Fig. 7d). This might lead to a better performance of the combination of solar and RoR from Cadipietra ($S_H = 1$) than the one of solar and RoR from Posina ($S_H = 0$) at 12 h and daily scales. Especially for the daily scale in which the difference is larger (from $WBCI_{Solar\text{-}Posina} = 0.17$ to $WBCI_{Solar\text{-}Cadipietra} = 0.25$) than for the 12 h scale (from $WBCI_{Solar\text{-}Posina} = 0.17$ to $WBCI_{Solar\text{-}Cadipietra} = 0.2$). This difference might be caused by the fact that snowmelt dominated streams display a daily periodicity in the spring and early summer seasons, which presents a time lag respect to solar radiation. This periodicity is however not present in rain dominated catchments.

Fig. 7b shows a 6 months WBCI peak that can be interpreted from the WTC (Fig. 7a) as the result of sporadic coherence with a π/2 time lag. In addition, the yearly peak is associated to an isolated time span in which the signals are in counter-phase. Focusing on the WBCI between solar energy and RoR Posina (Fig. 7d), we observe a high WBCI value (slightly larger than 0.6) at the 3–6 months scale. The two runoff peaks that characterize the hydrological regime of Posina normally occur in April and between October and December, while the maximum solar energy production takes place between June and August. This leads to a high complementarity between these two VRE sources during most of the year.

At the yearly scale we can observe low WBCI values (WBCI = 0.1) between solar and RoR from snow-dominated catchment (Fig. 7d), since both follow a similar yearly cycle triggered by solar radiation and temperature. On the contrary, higher WBCI values are detected for the complementarity between RoR from Posina with RoR from Cadipietra (WBCI = 0.32), and solar energy with RoR from Posina (WBCI = 0.33). Therefore, smoother temporal variability at yearly scale can be expected for these mix combinations.

The WBCI analysis points out the potential complementarity of the energy sources at different temporal scales. From the WTC and WBCI results in combination with the previous analysis of the input data (including the electricity demand), we might be able anticipate specific combinations that will show lower energy balance variance for the targeted scales of variability. However, the main purpose of the WTC and suggested index is to serve as screening tool to identify the potential complementarity of the VRE sources at multiple temporal scales. The subsequent assessment is therefore needed to fully understand the evolution of the energy balance variance for the different combinations at different temporal scales.

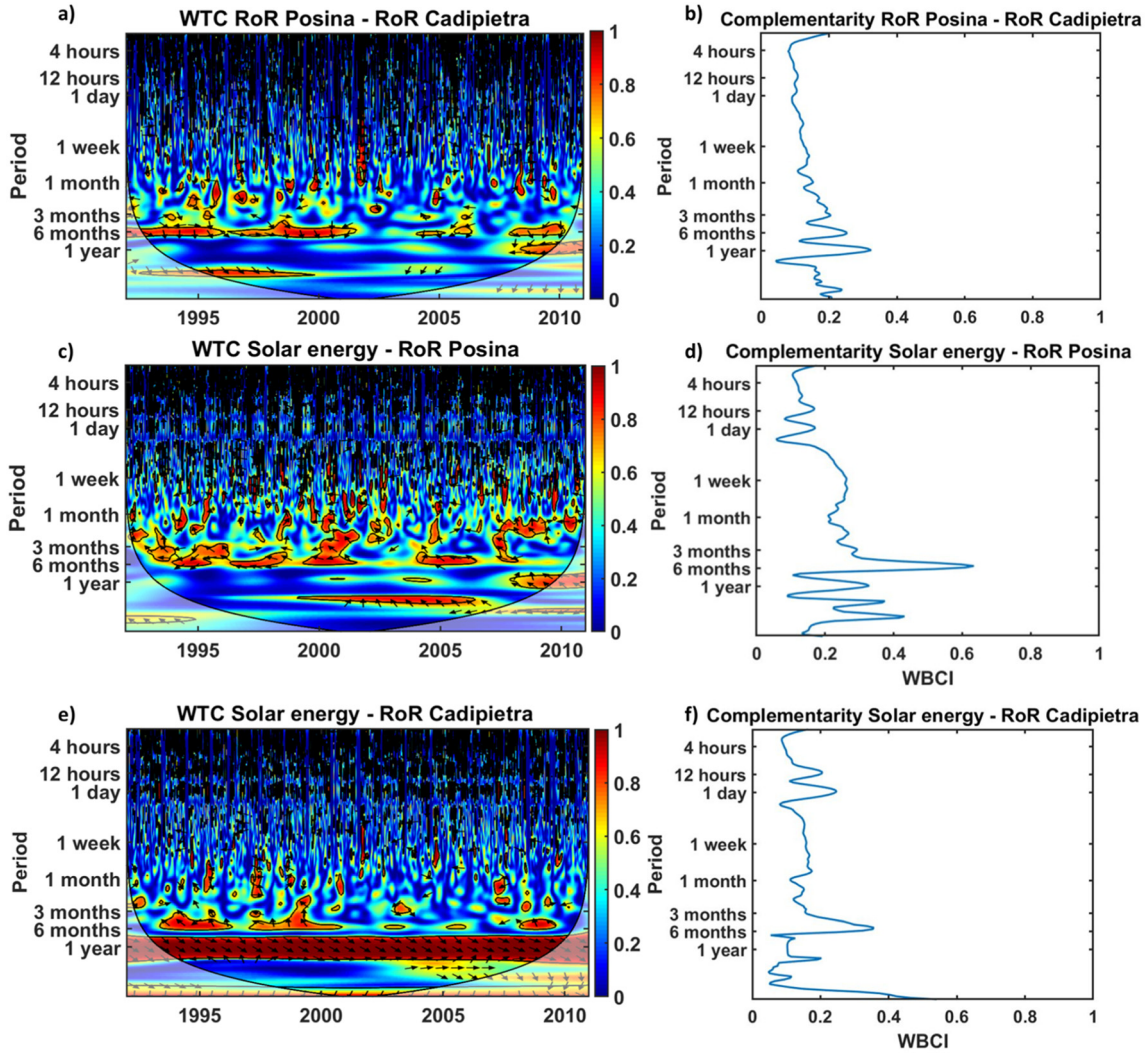

Fig. 7. Wavelet Transform Coherence (WTC) and wavelet-based complementarity index (WBCI) between run-of-the-river hydropower energy production from the rain dominated catchment and from the snow dominated catchment (plot a and b), between photovoltaic energy production and RoR hydropower energy production from the rain dominated catchment Posina (plot c and d), between photovoltaic energy production and RoR hydropower energy production from the snow dominated catchment Cadipietra (plot e and f). Blue color means no coherence between the variables (value equal to 0) and red color means total coherence (value equal to 1). Arrows show the relative angular phase relationships between analyzed signals. Right pointing arrows depict in-phase, while left pointing arrows represent anti-phase relationship. Vertically upward arrows depict a lead of π/2 or one-quarter (downward a lag) between analyzed signals. The WBCI highlights at which scales the variables show high complementarity.

4.2. Analysis of the energy balance at different temporal scales

Our study aims at investigating the energy balance at different temporal scales of a 100% renewable energies scenario, in which we consider the different combinations of photovoltaic (PV) and run-of-river (RoR) energy sources. In particular, the sensitivity studies explore 421 scenarios of energy mix defined by different sharing coefficients S_{PV} and S_H ranging from 0 to 1 using regular steps of 0.05. Note that when S_{PV} equals 1, S_H value does not matter and all the power generation comes from PV system only.

For this purpose, we compute the continuous wavelet transform (CWT) of the energy balance for the different combinations of the selected VRE sources. The CWT allows us to better understand the evolution of the energy balance signal for the different energy mix solutions, highlighting its relevant periodicities. Fig. 8 shows the CWT of the energy balance for the different considered combinations of VRE sources. The different columns show an increase in the amount of the solar power supplied to the system from 0% (on the left) to 100% (on the right). The different rows show the contribution to the total energy supply from rain or snow fed RoR. The top row contains only a combination of solar power and RoR generated in Cadipietra (snow dominated catchment) and the bottom row a combination of solar power and RoR generated in Posina (rain dominated catchment). In particular, $S_{PV} = 0$ and $S_H = 1$ represents the scenario for which 100% of the energy comes from the run-of-the-river hydropower plant of the snow dominated catchment (Cadipietra), while $S_{PV} = 0$ and $S_H = 0$ refers to the scenario for which 100% of the energy comes from the run-of-the-river hydropower plant of the rain dominated river basin (Posina).

Analyzing the results from left to right we can observe the effect of an increase in S_{PV}. This leads to a stronger daily signal with increase in non-stationarity at the daily and sub-daily scales (intermittent high wavelet power spots due to the seasonality of the solar cycle). We observe that the higher the S_{PV} contribution, the stronger the yearly periodicity. If we analyze the matrix of results from top to bottom, we can observe that the yearly signal is stronger and more focused in snow dominated catchments than in rain fed catchments. This is due to the fact that snow dominated catchments are characterized by strong seasonality and consequently a strong yearly cycle, while this is not present

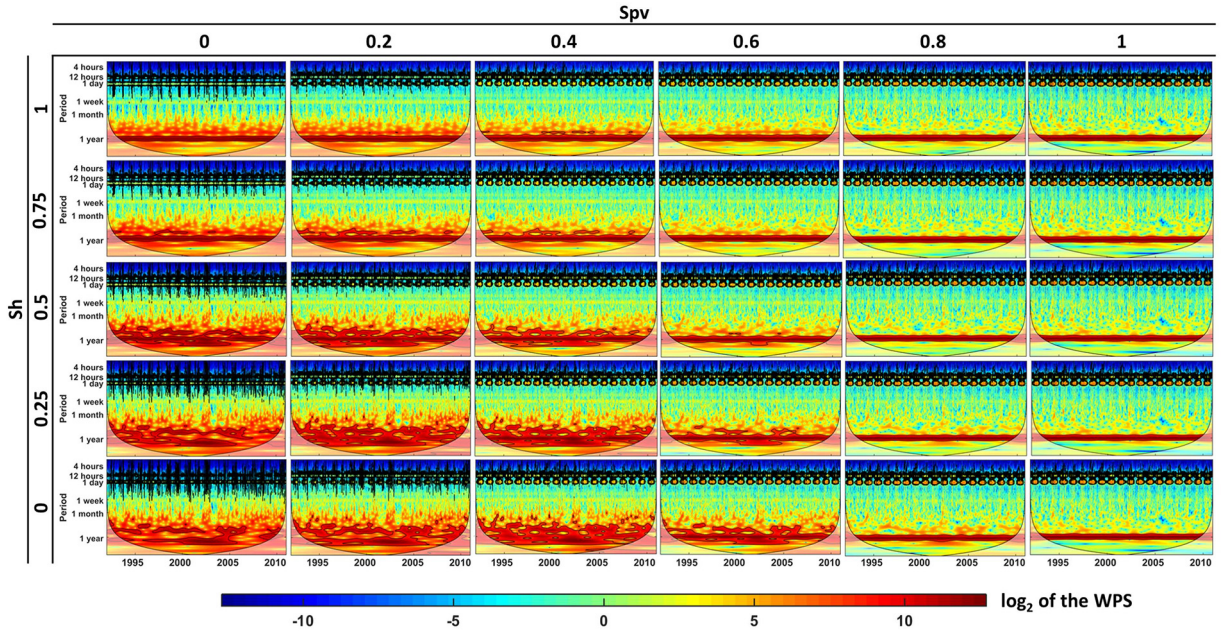

Fig. 8. CWT of the energy balance of the different combinations of energy mix considering percentage of photovoltaic energy production ($S_{PV} = 1$ implies 100% solar energy) and distribution of the remaining percentage between run-of-the river hydropower plants. S_H determines the share from a rain dominated catchment ($S_{PV} = 0$, $S_H = 0$ indicates 100% energy from run-of-the river rain dominated river basin) and snow dominated catchment ($S_{PV} = 0$, $S_H = 1$ indicates 100% energy from run-of-the river snow dominated river basin). The CWT spectrum shows time (years) on the ordered axis, and the analyzed scales (period) on the abscissa. Red colors represent high wavelet energy values (i.e., strong periodicity) blue colors represent low values of the wavelet power (i.e. weak periodicity).

for rain dominated catchments, as already observed in Figs. 2 and 3. From Fig. 8 we can detect the relevant temporal scales (i.e.: sub-daily, daily, and from seasonal to yearly scales) that are contributing the most to the energy balance fluctuations (under or/and over shooting). Additionally, although with lower wavelet power we observe a pattern that emerges at weekly scale.

To complement Fig. 8 and support our findings, we include Fig. 9 showing the variability of the energy balance for the different combinations of energy mix at different temporal scales. First, we show the variance values of the original signals and the signal constituted by the previously detected relevant temporal scales. We can observe that Fig. 9b represents fairly well the variance values of the original signal (Fig. 9a).

Secondly, in Fig. 9c–f we focus only on specific scales (i.e.: sub-daily, daily, weekly, and yearly) to better understand the energy balance variability. The variance values are computed from the decomposed signals obtained using DWT. The x- and y-axis represent the sharing coefficients S_{PV} and S_H, respectively.

In Fig. 9a we can observe that the original signal has minimum variance for $S_{PV} = 0.25$ and $S_H = 0.45$. We hence referred to this combination of energy sources as the optimal combination. Our objective now is to investigate at which scales this combination outperforms all other combinations. To achieve this goal, we quantify the variance for the different scales in which we can decompose the signal using DWT. We can observe that sub-daily and daily variance is lowest for S_{PV} values smaller than 0.1 and 0.2, respectively. The sub-daily scale variance values are non-dependent on the S_H value and increase almost linearly for increasing S_{PV} value. However, at the daily scale we observe that combinations with S_H larger than 0.2 (in addition to $S_{PV} < 0.2$) have the best performance (minimum energy balance variance values). At the weakly scale (Fig. 9e) we can observe that the range of variance values (from 0 to 0.05) is much smaller than for the other scales. This is due to the fact that the weekly signal is not a dominant scale in our time series, as it was shown the energy balance CWT analysis (Fig. 8). It is noteworthy that storage driven hydropower plants are however characterized by this weekly periodicity (Pérez Ciria et al., 2019), triggered, in turn, by the weekly variability of the electricity demand. Focusing on larger scales, to assess the wider range of dominant scales we computed the variance of the summation of the decomposed signals from 3 months to one year for the DWT analysis (implicitly considering also the dominant 6 months scale), which we referred to as the yearly variance (Fig. 9f). This yearly variance distribution in the S_H–S_{PV} plane displays a minimum at the point of coordinates (0.55, 0.1).

To finalize our analysis, we determine the dominant scale of variability (i.e.: scale at which we find the maximum variance value) for the different combinations (Fig. 10a), and the variance values of this specific dominant scale (Fig. 10b). Additionally, we investigate the evolution of the variance at different temporal scales for a given S_{PV} (Fig. 10c) and S_H value (Fig. 10d), selected from the optimal combination coordinates ($S_{PV} = 0.25$ and $S_H = 0.45$).

5. Discussion

5.1. Input data CWT and WTC analysis

The continuous wavelet transform (CWT) analysis shows that the selected variable renewable energy (VRE) sources behave significantly different at multiple temporal scales. This different behavior among the potential energy sources implies a high degree of flexibility for the different energy combinations, which is a prerequisite to satisfy efficiently the electricity demand (high complementarity). In addition, the analysis gives us the possibility to understand the targeted scales of variability and detect which temporal scales might not be satisfied with any of the available combinations.

First, the electricity demand is characterized by a strong sub-daily and daily variability that we can easily recognize in the global wavelet spectrum (GWS) (Fig. 3d). The RoR energy production of the rain dominated catchment does not show a strong daily pattern (Fig. 4). In contrast, the daily periodicity is consistent for the RoR energy of the snow dominated catchment. The peak associated to the daily periodicity is

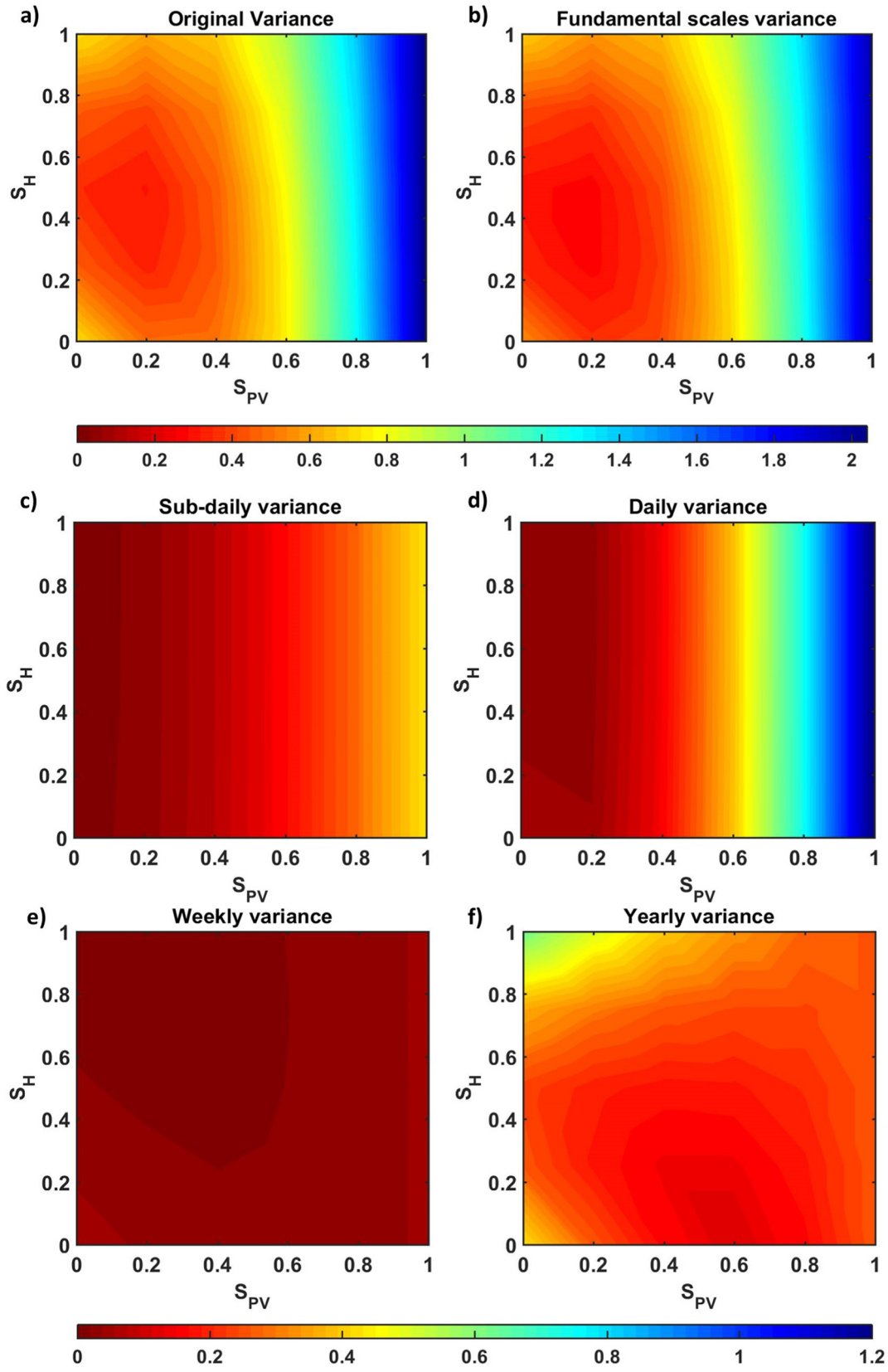

Fig. 9. Variability of the balance between energy load and supply of the different combinations of energy mix computed from the signal decomposition using DWT. The x- and y-axis represent the sharing coefficients S_{PV} and S_H, respectively. The color map gives the variance value of the energy balance (scaled values) for a specific temporal scale or range of temporal scales. First, plots a) and b) show the variance of the original signal, and fundamental scales (including sub-daily, daily, and from seasonal to yearly), respectively (color scale ranging from 0 to 2). Secondly, plots c-f show the variance at c) sub-daily, d) daily, e) weekly, and f) yearly scale (with variance values ranging from 0 to 1.2).

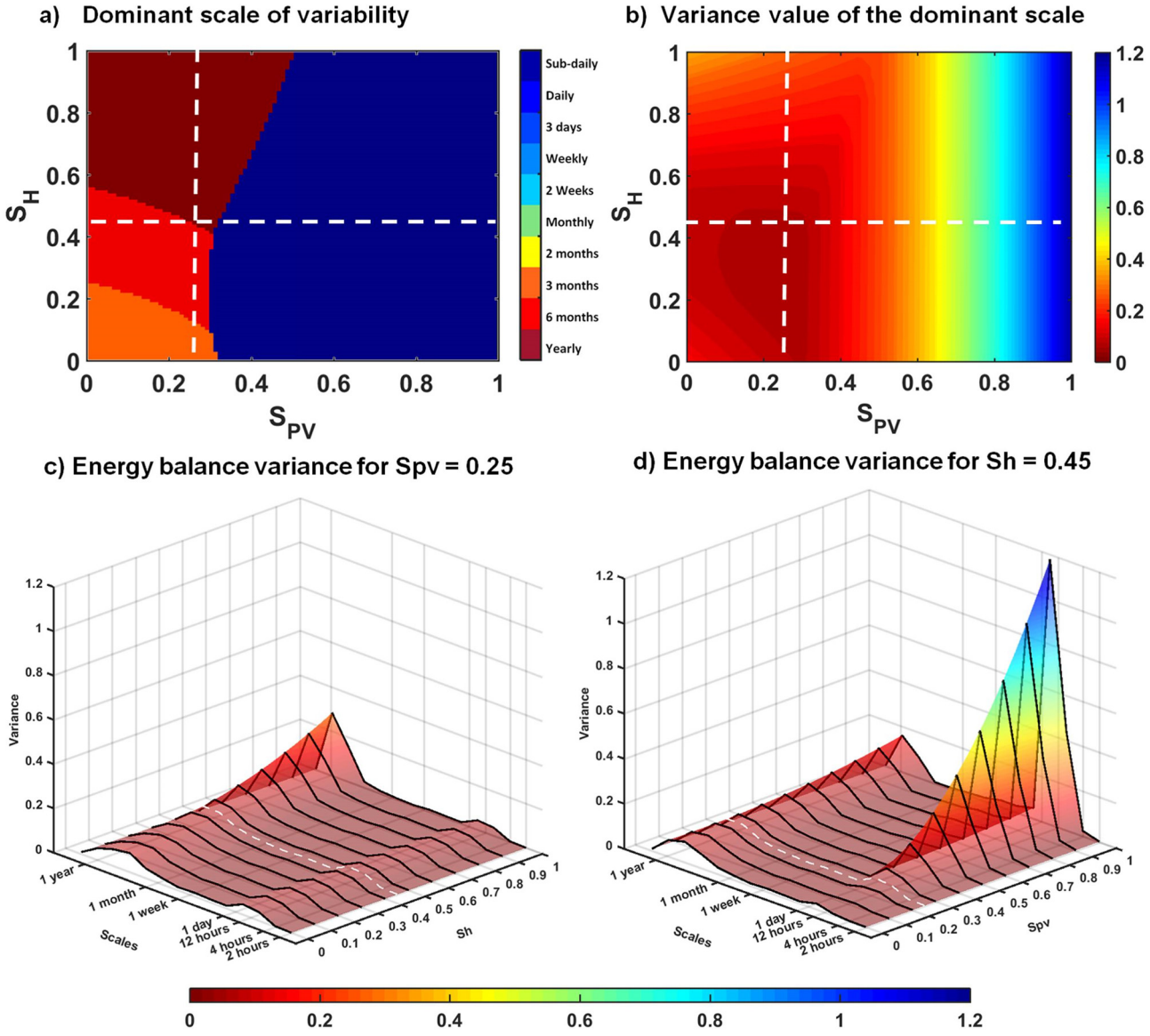

Fig. 10. Variance of the energy balance at different temporal scales determined applying DWT. Plot a) shows the dominant scales of variability (temporal scale at which we find the maximum variance value for a given combination); plot b) displays the value of the maximum variance observed at the specific scale given in plot b; plot c) and d) show the evolution of the variance at different temporal scales for $S_{PV} = 0.25$ and $S_H = 0.45$, respectively. In plot b, c, and d the color indicates the variance value and ranges from red (variance equal to 0) to blue (variance equal to 1.2).

detectable in the GWS (Fig. 5d). This periodicity is intermittent and only present when melting processes are ongoing. The rate of melting of snow and ice, which is predominantly controlled by the solar radiation intensity, determines runoff diurnal cycle. Both sub-daily and daily scales of variability are present for solar energy production. However, when focusing on the wavelet power spectrum (WPS) (Fig. 6c) we can observe that this signal is intermittent presenting discontinuities during the winter period when the solar energy production reaches its minimum productivity throughout the year. A similar pattern occurs for the sub-daily scale. It is noteworthy to mention that the diurnal cycle of photovoltaic energy has a more extreme behavior with no energy production at night, while the demand has a smoother behavior (Fig. 6b). This fact highlights the necessity of a combination of VRE sources, which is dependent on the temporal scale and non-stationary in time (significant seasonality).

Secondly, a 3 days and weekly pattern emerge in the WPS of the electricity demand due to higher electricity consumption during the weekdays. This weekly cycle is strictly linked to human activities and cannot be reproduced by RoR or photovoltaic energy production. In order to mimic this signal additional energy sources, such as hydropower plants with storage capacity or the use of batteries, would need to be introduced for a 100% renewable energies scenario. The present analysis might be useful to optimize reservoir capacity and adapt management strategies of such hydropower plants to reduce the negative impacts associated to hydropeaking. Furthermore, we detected a 3–-6 months periodicity in the electricity demand associated to winter (heating) and summer (cooling) peaks. To cover this periodicity the presence in the energy mix of the RoR from the rain dominated catchment becomes relevant, giving a higher degree of flexibility throughout the year. Finally, although present during the whole analyzed time span, the yearly periodicity shows an irregular behavior in terms of wavelet power intensity. This is not the case for RoR from a snow dominated catchment and photovoltaic energy, both showing a strong and continuous yearly periodicity. From Figs. 3–6 we are able to anticipate that due to the significance of the daily cycle for the electricity demand, the share of the photovoltaic energy might play a more relevant role in the mix.

From a global perspective taking into consideration the whole analyzed time span, the RoR energy sources might provide a more reliable energy supply than the solar energy, since photovoltaic energy is characterized by a strong seasonality and null values at night and during cloudy days. However, it is also clear that a combination of the three energy sources will grant the optimal and most efficient solution.

The wavelet transform coherence (WTC) analysis shows high and low coherence values among the selected renewable energies as indicator of potential complementarity. The WTC depicts with high coherence values and arrows pointing to the right (in phase) the temporal scales at which both energy sources have a similar periodicity. The WTC between RoR energy production from Posina (representing rain fed catchments) and RoR hydro from Cadipietra (snow dominated catchment) presents low coherence values in general and only sporadic high coherence with a time lag between signals (Fig. 7a). Similar results are obtained for RoR from Posina and solar energy (Fig. 7c). Both low coherence values and high coherence with a phase shift present an opportunity for high complementarity and consequently an increase in energy balance effectivity. Only the WTC between solar energy and RoR energy from Cadipietra shows a stationary high coherence at yearly scale, since the solar radiation directly affects both solar energy production and the hydrological cycle of snow dominated catchments.

The introduced wavelet-based complementarity index (WBCI) considers coherence values and phase lag between variables providing therefore a holistic assessment of the complementarity between energy sources at multiple temporal scales. At the sub-daily and daily scales, both RoR from Posina and Cadipietra show similar WBCI values in combination with solar energy (Fig. 7d and f). However, the highest WBCI values at sub-daily and daily scales, implying higher complementarity and therefore better performance, were detected for the combination between solar energy and RoR from Cadipietra (Fig. 7f). This small difference is confirmed in the energy balance variance analysis (Fig. 9c and d). A closer look reveals that with the same percentage of solar power, a higher share of RoR from Cadipietra has lower energy balance variance values at sub-daily and especially at daily scale. We can observe that at daily scale the lowest variance values are only achieved for $S_H > 0.1$.

Moreover, at the yearly scale we observed low WBCI values between solar and RoR from snow-dominated catchment (Fig. 7f). Similar WBCI values were detected for the complementarity between RoR from Posina with RoR from Cadipietra (Fig. 7b), and RoR from Posina with solar energy (Fig. 7d) with WBCI = 0.32 and WBCI = 0.33, respectively. These findings are in line with the results obtained for the energy balance variance at yearly scale (Fig. 9f), in which the best performance (lowest energy balance variance) appears for the combination of RoR from Posina with solar energy (which had the highest WBCI = 0.33). Low energy balance variance values at the yearly scale are also associated to the combination of RoR from Posina with RoR from Cadipietra ($S_H = 0.5$) for the different shares of solar energy. Combinations of $S_H = 1$ and different S_{PV} values presented, in turn, the highest energy balance variance values (Fig. 9f). Thus, the WTC analysis reveals that the share of RoR from the rain dominated catchment plays a relevant role in the energy mix complementarity, especially at the yearly scale.

5.2. Energy balance of the energy mix combinations

The energy balance CWT analysis is used to assess the complementarity of the different renewable energies (Fig. 8). We carried out an analysis exploring 30 mix scenarios covering the full range of PV and RoR ratios of S_{PV} and S_H. The CWT gives us the possibility to assess at a glance the complementarity of the VRE sources and the suitability of the energy mix combinations at various temporal scales (from sub-daily to yearly scale). This type of analysis also allows us to explore the evolution of the signal behavior at different temporal scales.

We can first observe in Fig. 8 that combinations with a share of photovoltaic energy higher than 60% (S_{PV} = 0.6, 0.8, and 1) have a prominent discontinuity in sub-daily and daily scales. This illustrates that energy mix combinations with high share of solar energy do not cover electricity demand at night, and neither during cloudy periods. In fact, if we only focus on the daily scale, a stationary signal (continuous pattern without discontinuities) in energy balance is observed for the combinations with $S_{PV} = 0$ (no presence of solar energy in the mix). In addition, Fig. 9c and d show that the lowest variance values of the decomposed signals at the sub-daily and daily scales are for the combinations with no solar energy contribution. In particular, Fig. 9c and d show that a 20% of photovoltaic energy is enough to mimic the daily cycle of the electricity demand, while the contribution of RoR energy supply is needed to cover the electricity demand at night.

If we focus on the weekly scale, we observe that although a pattern is present in the energy balance CWTs (Fig. 8), no high wavelet power is associated to this periodicity (color ranges from green to yellow indicating values between 2 and 3 of the $\log_2$ (WPS)). In Fig. 9e we observe that the highest variance values at weekly scale are associated to 100% photovoltaic energy supply ($S_{PV} = 1$) and 100% of RoR from rain dominated catchment ($S_H = 0$, $S_{PV} = 0$). However, the computed variance values for the weekly scale (Fig. 9e) are two orders of magnitude lower than the original variance (Fig. 9a). This confirms that the significance of the weekly scale is minor for the comparison of different energy mix combinations composed of RoR and PV. Weekly variance values of the energy balance might be even lower if we consider storage hydropower for instance.

For the yearly variance we observed in the input data analysis that the electricity demand time series does not present a particularly strong periodicity, as it is the case for the streamflow of the snow dominated catchment and the photovoltaic energy. On the contrary, a wider spectrum of scales (from monthly to yearly) seems to present high wavelet power values (red area in Fig. 3c). The variance of the yearly scale for the DWT analysis (Fig. 9f) is the summation of the decomposed signals from 3 months to one year, which is why although photovoltaic and RoR from snow fed catchment succeed in covering the yearly scale, fail to satisfy the wider range of scales that are demonstrated to be significant for the electricity demand (Fig. 3). This is true especially for solar energy, which shows very low wavelet power at temporal scales immediately smaller than the yearly scale (Fig. 6), while a completely different pattern is present for the electricity demand. In our study, the only renewable source that shows a wider spectrum of high wavelet power with no dominant periodicity is the RoR from the rain dominated catchment. However, the distribution of discontinuities is associated to precipitation events and does not fully correspond with the discontinuities present in the CWT of the electricity demand. Therefore, a mixture of the available energy sources achieves the best performance for this range of scales. We can therefore conclude that different sources comply with the electricity demand for different temporal scales and different periods of the year.

5.3. Advantages and limitations of the proposed method

The suggested methodology can only be successfully implemented if a minimum time series length with hourly resolution is available. This requirement must be met to obtain statistical significant results out of the cone of influence (COI). The proposed methodology presents also several advantages in comparison to other available methods. One of its main strengths is that we have the possibility to address different temporal scales without losing any piece of information, unlike might happen when using temporal aggregation. Secondly, we are able to find the most relevant temporal scales for the electricity demand and establish them as target temporal scales (the ones associated with the largest variability). Additionally, we are able to detect temporal scales that although not the main drivers of variability, still play a role (e.g.: weekly).

The wavelet analyses (CWT, WTC, WBCI, and DWT) of the available VRE sources allow us to identify at which temporal scales the electricity

demand can be satisfied by one or a mix of the renewable sources considered. The information revealed by the WTC and especially by the WBCI, which includes coherence values and phase lag computed for each scale, assists us in the detection of the scales for which the analyzed variables show on average low or high complementarity at multiple temporal scales. Furthermore, we can detect the limitations of the energy mix combinations to mimic patterns that are associated to specific temporal scales (e.g.: weekly) that do not naturally emerge in any of the renewable sources considered. In our case study, to mimic the demand signal at the weekly scale, we would need to rely on additional energy sources, such as hydropower plants using dams as storage facilities.

The analysis explicitly permits to relate energy balance variations at different temporal scales to the time-varying characteristics of the geophysical processes and the electricity demand. We apply wavelet analysis to disclose the crucial periodicities of a signal and to determine their alterations, if present, in time. Our study area shows a rather stationary behavior during the whole analyzed time span (from 1992 to 2012). However, wavelet analysis allows us to detect changes (i.e.: breakpoints or trends) of the analyzed time series. These changes might lead us to a better understanding of trends of the different signals and contribute to more sophisticated predictions.

More specifically, while focusing on the climate variables, changes in temperature, precipitation and glacier coverage affecting changes in the time series patterns of VREs production (Bonato et al., 2019; François et al., 2018; Puspitarini et al., 2020), can be identified and therefore taken into account in further studies (e.g.: included in simulations of different energy mix combinations). In addition, climate change impacts might directly affect socioeconomic factors, such us electricity demand (Gaudard et al., 2014; Maran et al., 2014; Ravazzani et al., 2016). One additional advantage of our method regarding further research is that allows us to increase the complexity of the mixing (i.e.: including additional renewable energy sources) and still be able to detect the relevant temporal scales at a glance.

6. Conclusions

In this work, we consider the performance of 100% renewable energy supply scenarios. This study investigates the structure of the complementarity at multiple temporal scales between run-of-river (RoR) hydro and solar photovoltaic (PV) power in an alpine transect located in the North of Italy. We applied various wavelet analyses to assess the energy mix combinations and the driving mechanisms behind the energy sources complementarity. The input data analysis represents an indispensable step to better understand the temporal structure of the energy sources and the electricity demand time series. The CWT does not only show the relevant periodicities that characterize each time series, but might aid in the detection of intermittent patterns, such as sub-daily and daily energy production and electricity consumption patterns that significantly change over the year (especially relevant in Nordic countries) or alterations in time of the signal behavior (e.g.: sudden changes in the signal variability due to climatic forcing or socioeconomic triggers).

The WTC analysis among the selected VRE sources serves as indicator of potential complementarity and allows us to detect non-stationary behaviors. Based on the WTC, we introduce a new metric to assess the complementarity between VRE sources across the continuous range of temporal scales, the wavelet-based complementarity index (WBCI). We show that this index varies at different temporal scales and it helps explaining the discrepancy between demand and supply in the study area. Moreover, the CWT and DWT-variance analyses allow us to anticipate optimal energy sources combinations. Using wavelet transform we analyze the performance of the mix scenarios to determine the optimal energy mix for the selected study area at specific temporal scales. The signal behavior differs from short time scales (i.e. sub-daily, daily, weekly scales) to large temporal scales (i.e.: monthly, seasonal, 6 months, and yearly scales). Short time scales are relevant mainly due to the diurnal cycle of PV, but also due to the daily pattern of the electricity demand. In turn, variability at large temporal scales has proved to be a good index for assessing the storage requirement. Combining different renewable energy sources is beneficial due to their complementarity in time, which limits the energy production and load balance variability. The most efficient energy mix needs minimum balancing costs (i.e.: minimizing investments in over-capacity or transmission capacity) and storage needs (i.e.: optimizing reservoirs volume and batteries). Our findings can contribute to the proper development of further studies addressing the optimization of 100% renewable energy scenarios. Thus, the applied wavelet based analyses offer a robust framework for practical renewable energy balance studies. In particular, our analysis might be especially interesting for regions where the temporal scales of the dominant periodicities have not been identified yet or where dominant periodicities significantly change over the year (e.g.: in Nordic region). As a potential future research stemming from this one, the developed methodology could be applied using longer time series so that we could also detect potential complementarity at large temporal scales and analyze the influence of climate patterns on VRE.

CRediT authorship contribution statement

T. Pérez Ciria: Conceptualization, Methodology, Software, Validation, Formal analysis, Writing - original draft, Visualization. **H.D. Puspitarini:** Data curation, Resources, Software, Validation, Writing - review & editing. **G. Chiogna:** Conceptualization, Methodology, Validation, Formal analysis, Writing - review & editing, Supervision, Funding acquisition. **B. François:** Validation, Writing - review & editing. **M. Borga:** Conceptualization, Methodology, Validation, Writing - review & editing, Supervision, Project administration, Funding acquisition.

Declaration of competing interest

The authors declare that they have no known competing financial interests or personal relationships that could have appeared to influence the work reported in this paper.

Acknowledgements

The first author acknowledges funding from the Doktoratsstipendium aus der Nachwuchsförderung from the University of Innsbruck, and its partnership with the University of Padova. The second author acknowledges funding support by LPDP (Indonesia Endowment Fund for Education), Ministry of Finance, the Republic of Indonesia. G.C. acknowledges the support of the Stiftungsfonds für Umweltökonomie und Nachhaltigkeit GmbH (SUN).

Appendix A. Supplementary data

Supplementary data to this article can be found online at https://doi.org/10.1016/j.scitotenv.2020.140179.

References

Alam, M.M., Rehman, S., Al-Hadhrami, L.M., Meyer, J.P., 2014. Extraction of the inherent nature of wind speed using wavelets and FFT. Energy for Sustainable Development 22, 34–47. https://doi.org/10.1016/j.esd.2014.02.004.

Balbastre-Soldevila, García-Bartual, Andrés-Doménech, 2019. A comparison of design storms for urban drainage system applications. Water 11 (4), 757. https://doi.org/10.3390/w11040757.

Beluco, A., Risso, A., Canales, F.A., 2019. Simplified evaluation of energetic complementarity based on monthly average data. MethodsX 6, 1194–1198. https://doi.org/10.1016/j.mex.2019.05.019.

Bonato, M., Ranzani, A., Patro, E.R., Gaudard, L., De Michele, C., 2019. Water-energy nexus for an Italian storage hydropower plant under multiple drivers. Water 11 (9), 1838. https://doi.org/10.3390/w11091838.

Bonkaney, A.L., Seidou Sanda, I., Balogun, A.A., 2019. Wavelet analysis of daily energy demand and weather variables. Journal of Energy 2019, 1–7. https://doi.org/10.1155/2019/4974107.

Borba, E.M., Brito, R.M., 2017. An index assessing the energetic complementarity in time between more than two energy resources. Energy Power Eng. 9 (9), 505–514. https://doi.org/10.4236/epe.2017.99035.

Brown, T., Schlachtberger, D., Kies, A., Schramm, S., Greiner, M., 2018. Synergies of sector coupling and transmission reinforcement in a cost-optimised, highly renewable European energy system. Energy 160, 720–739. https://doi.org/10.1016/j.energy.2018.06.222.

Canales, F.A., Jurasz, J., Beluco, A., Kies, A., 2020. Assessing temporal complementarity between three variable energy sources through correlation and compromise programming. Energy 192, 116637. https://doi.org/10.1016/j.energy.2019.116637.

Carey, S.K., Tetzlaff, D., Buttle, J., Laudon, H., McDonnell, J., McGuire, K., Seibert, J., Soulsby, C., Shanley, J., 2013. Use of color maps and wavelet coherence to discern seasonal and interannual climate influences on streamflow variability in northern catchments. Water Resour. Res. 49 (10), 6194–6207. https://doi.org/10.1002/wrcr.20469.

Chang, T.-P., Liu, F.-J., Ko, H.-H., Huang, M.-C., 2017. Oscillation characteristic study of wind speed, global solar radiation and air temperature using wavelet analysis. Appl. Energy 190, 650–657. https://doi.org/10.1016/j.apenergy.2016.12.149.

Chiogna, G., Marcolini, G., Liu, W., Pérez Ciria, T., Tuo, Y., 2018. Coupling hydrological modeling and support vector regression to model hydropeaking in alpine catchments. Sci. Total Environ. 633, 220–229. https://doi.org/10.1016/j.scitotenv.2018.03.162.

Chowdhury, A.F.M.K., Kern, J., Dang, T.D., Galelli, S., 2020. PowNet: a network-constrained unit commitment/economic dispatch model for large-scale power systems analysis. Journal of Open Research Software 8. https://doi.org/10.5334/jors.302.

Clerjon, A., Perdu, F., 2019. Matching intermittency and electricity storage characteristics through time scale analysis: an energy return on investment comparison. Energy Environ. Sci. 12 (2), 693–705. https://doi.org/10.1039/C8EE01940A.

Engeland, K., Borga, M., Creutin, J.-D., François, B., Ramos, M.-H., Vidal, J.-P., 2017. Space-time variability of climate variables and intermittent renewable electricity production – a review. Renew. Sust. Energ. Rev. 79, 600–617. https://doi.org/10.1016/j.rser.2017.05.046.

François, B., Borga, M., Anquetin, S., Creutin, J.D., Engeland, K., Favre, A.C., Hingray, B., Ramos, M.H., Raynaud, D., Renard, B., Sauquet, E., Sauterleute, J.F., Vidal, J.P., Warland, G., 2014. Integrating hydropower and intermittent climate-related renewable energies: a call for hydrology. Hydrol. Process. 28 (21), 5465–5468. https://doi.org/10.1002/hyp.10274.

François, B., Borga, M., Creutin, J.D., Hingray, B., Raynaud, D., Sauterleute, J.F., 2016a. Complementarity between solar and hydro power: sensitivity study to climate characteristics in Northern-Italy. Renew. Energy 86, 543–553. https://doi.org/10.1016/j.renene.2015.08.044.

François, B., Hingray, B., Raynaud, D., Borga, M., Creutin, J.D., 2016b. Increasing climate-related-energy penetration by integrating run-of-the river hydropower to wind/solar mix. Renew. Energy 87, 686–696. https://doi.org/10.1016/j.renene.2015.10.064.

François, B., Martino, S., Tøfte, L., Hingray, B., Mo, B., Creutin, J.-D., 2017a. Effects of increased wind power generation on mid-Norway's energy balance under climate change: a market based approach. Energies 10 (2), 227. https://doi.org/10.3390/en10020227.

François, B., Zoccatelli, D., Borga, M., 2017b. Assessing small hydro/solar power complementarity in ungauged mountainous areas: a crash test study for hydrological prediction methods. Energy https://doi.org/10.1016/j.energy.2017.03.090.

François, Baptiste, Hingray, B., Borga, M., Zoccatelli, D., Brown, C., Creutin, J.-D., 2018. Impact of climate change on combined solar and run-of-river power in northern Italy. Energies 11 (2), 290. https://doi.org/10.3390/en11020290.

Fu, C., James, A.L., Wachowiak, M.P., 2012. Analyzing the combined influence of solar activity and El Niño on streamflow across southern Canada. Water Resour. Res. 48 (5). https://doi.org/10.1029/2011WR011507.

García-Bartual, R., Andrés-Doménech, I., 2017. A two-parameter design storm for Mediterranean convective rainfall. Hydrol. Earth Syst. Sci. 21 (5), 2377–2387. https://doi.org/10.5194/hess-21-2377-2017.

Gaudard, L., Romerio, F., Dalla Valle, F., Gorret, R., Maran, S., Ravazzani, G., Volonterio, M., 2014. Climate change impacts on hydropower in the Swiss and Italian Alps. Sci. Total Environ. 493, 1211–1221. https://doi.org/10.1016/j.scitotenv.2013.10.012.

Grinsted, A., Moore, J.C., Jevrejeva, S., 2004. Application of the cross wavelet transform and wavelet coherence to geophysical time series. Nonlinear Process. Geophys. 11 (5/6), 561–566. https://doi.org/10.5194/npg-11-561-2004.

GSE, 2019. Rapporto delle Attivita 2018. Retrieved from. https://www.gse.it/documenti_site/DocumentiGSE/Rapporti delle attività/GSE_RA2018.pdf.

Guan, K., Thompson, S.E., Harman, C.J., Basu, N.B., Rao, P.S.C., Sivapalan, M., Packman, A.I., Kalita, P.K., 2011. Spatiotemporal scaling of hydrological and agrochemical export dynamics in a tile-drained Midwestern watershed. Water Resour. Res. 47 (10). https://doi.org/10.1029/2010WR009997.

Han, S., Zhang, L.-n., Liu, Y.-q., Zhang, H., Yan, J., Li, L., et al., 2019. Quantitative evaluation method for the complementarity of wind–solar–hydro power and optimization of wind–solar ratio. Appl. Energy 236, 973–984.

Heide, D., von Bremen, L., Greiner, M., Hoffmann, C., Speckmann, M., Bofinger, S., 2010. Seasonal optimal mix of wind and solar power in a future, highly renewable Europe. Renew. Energy 35 (11), 2483–2489. https://doi.org/10.1016/j.renene.2010.03.012.

IEA, 2018. Electricity information: overview. Retrieved from. https://webstore.iea.org/download/direct/2261?fileName=Electricity_Information_2018_Overview.pdf.

Jacobson, M.Z., Delucchi, M.A., 2011. Providing all global energy with wind, water, and solar power, part I: technologies, energy resources, quantities and areas of infrastructure, and materials. Energy Policy 39 (3), 1154–1169. https://doi.org/10.1016/j.enpol.2010.11.040.

Jurasz, J., Canales, F.A., Kies, A., Guezgouz, M., Beluco, A., 2020. A review on the complementarity of renewable energy sources: concept, metrics, application and future research directions. Sol. Energy 195, 703–724. https://doi.org/10.1016/j.solener.2019.11.087.

Kies, A., Schyska, B.U., von Bremen, L., 2016. The optimal share of wave power in a highly renewable power system on the Iberian Peninsula. Energy Rep. 2, 221–228. https://doi.org/10.1016/j.egyr.2016.09.002.

Kougias, I., Szabó, S., Monforti-Ferrario, F., Huld, T., Bódis, K., 2016. A methodology for optimization of the complementarity between small-hydropower plants and solar PV systems. Renew. Energy 87, 1023–1030. https://doi.org/10.1016/J.RENENE.2015.09.073.

Kratzert, F., Klotz, D., Brenner, C., Schulz, K., Herrnegger, M., 2018. Rainfall–runoff modelling using long short-term memory (LSTM) networks. Hydrol. Earth Syst. Sci. 22 (11), 6005–6022. https://doi.org/10.5194/hess-22-6005-2018.

Labat, D., 2006. Oscillations in land surface hydrological cycle. Earth Planet. Sci. Lett. 242 (1–2), 143–154. https://doi.org/10.1016/j.epsl.2005.11.057.

Labat, David, 2010. Cross wavelet analyses of annual continental freshwater discharge and selected climate indices. J. Hydrol. 385 (1–4), 269–278. https://doi.org/10.1016/j.jhydrol.2010.02.029.

Labat, D., Ababou, R., Mangin, A., 2000. Rainfall–runoff relations for karstic springs. Part II: continuous wavelet and discrete orthogonal multiresolution analyses. J. Hydrol. 238 (3–4), 149–178. https://doi.org/10.1016/S0022-1694(00)00322-X.

Labat, David, Ronchail, J., Callede, J., Guyot, J.L., De Oliveira, E., Guimarães, W., 2004. Wavelet analysis of Amazon hydrological regime variability. Geophys. Res. Lett. 31 (2). https://doi.org/10.1029/2003GL018741.

Maheswaran, R., Khosa, R., 2012. Comparative study of different wavelets for hydrologic forecasting. Comput. Geosci. 46, 284–295. https://doi.org/10.1016/j.cageo.2011.12.015.

Maran, S., Volonterio, M., Gaudard, L., 2014. Climate change impacts on hydropower in an alpine catchment. Environ. Sci. Pol. 43, 15–25. https://doi.org/10.1016/j.envsci.2013.12.001.

Marcolini, G., Bellin, A., Disse, M., Chiogna, G., 2017. Variability in snow depth time series in the Adige catchment. Journal of Hydrology: Regional Studies 13, 240–254. https://doi.org/10.1016/j.ejrh.2017.08.007.

Ming, B., Liu, P., Cheng, L., Zhou, Y., Wang, X., 2018. Optimal daily generation scheduling of large hydro–photovoltaic hybrid power plants. Energy Convers. Manag. 171, 528–540. https://doi.org/10.1016/J.ENCONMAN.2018.06.001.

Moore, R.J., 2007. The PDM rainfall-runoff model. Hydrol. Earth Syst. Sci. 11 (1), 483–499. https://doi.org/10.5194/hess-11-483-2007.

Moser, D., Vettorato, D., Vaccaro, R., Del Buono, M., Sparber, W., 2014. The PV potential of South Tyrol: an intelligent use of space. Energy Procedia 57, 1392–1400. https://doi.org/10.1016/j.egypro.2014.10.130.

Nalley, D., Adamowski, J., Khalil, B., 2012. Using discrete wavelet transforms to analyze trends in streamflow and precipitation in Quebec and Ontario (1954–2008). J. Hydrol. 475, 204–228. https://doi.org/10.1016/j.jhydrol.2012.09.049.

Nalley, D., Adamowski, J., Khalil, B., Biswas, A., 2016. Inter-annual to inter-decadal streamflow variability in Quebec and Ontario in relation to dominant large-scale climate indices. J. Hydrol. 536, 426–446. https://doi.org/10.1016/j.jhydrol.2016.02.049.

Norbiato, D., Borga, M., Merz, R., Blöschl, G., Carton, A., 2009. Controls on event runoff coefficients in the eastern Italian Alps. J. Hydrol. 375 (3–4), 312–325. https://doi.org/10.1016/j.jhydrol.2009.06.044.

Pérez Ciria, T., Chiogna, G., 2020. Intra-catchment comparison and classification of long-term streamflow variability in the Alps using wavelet analysis. J. Hydrol. 587, 124927.

Pérez Ciria, T., Labat, D., Chiogna, G., 2019. Detection and interpretation of recent and historical streamflow alterations caused by river damming and hydropower production in the Adige and inn river basins using continuous, discrete and multiresolution wavelet analysis. J. Hydrol. 578, 124021. https://doi.org/10.1016/j.jhydrol.2019.124021.

Puspitarini, H.D., François, B., Zaramella, M., Brown, C., Borga, M., 2020. The impact of glacier shrinkage on energy production from hydropower-solar complementarity in alpine river basins. Sci. Total Environ. 719, 137488. https://doi.org/10.1016/j.scitotenv.2020.137488.

Rathinasamy, M., Khosa, R., Adamowski, J., Ch, S., Partheepan, G., Anand, J., Narsimlu, B., 2014. Wavelet-based multiscale performance analysis: an approach to assess and improve hydrological models. Water Resour. Res. 50 (12), 9721–9737. https://doi.org/10.1002/2013WR014650.

Ravazzani, G., Dalla Valle, F., Gaudard, L., Mendlik, T., Gobiet, A., Mancini, M., 2016. Assessing climate impacts on hydropower production: the case of the Toce River basin. Climate 4 (2), 16. https://doi.org/10.3390/cli4020016.

Raynaud, D., Hingray, B., François, B., Creutin, J.D., 2018. Energy droughts from variable renewable energy sources in European climates. Renew. Energy 125, 578–589. https://doi.org/10.1016/J.RENENE.2018.02.130.

Roldán Fernández, J.M., Burgos Payán, M., Riquelme Santos, J.M., Trigo García, Á.L., 2016. Renewable generation versus demand-side management. A comparison for the Spanish market. Energy Policy 96, 458–470. https://doi.org/10.1016/j.enpol.2016.06.014.

Schaefli, B., Maraun, D., Holschneider, M., 2007. What drives high flow events in the Swiss Alps? Recent developments in wavelet spectral analysis and their application to hydrology. Adv. Water Resour. 30 (12), 2511–2525. https://doi.org/10.1016/j.advwatres.2007.06.004.

Staffell, I., Pfenninger, S., 2018. The increasing impact of weather on electricity supply and demand. Energy 145, 65–78. https://doi.org/10.1016/J.ENERGY.2017.12.051.

Tiwari, M.K., Adamowski, J., 2013. Urban water demand forecasting and uncertainty assessment using ensemble wavelet-bootstrap-neural network models. Water Resour. Res. 49 (10), 6486–6507. https://doi.org/10.1002/wrcr.20517.

Torrence, C., Compo, G.P., 1998. A practical guide to wavelet analysis. Bull. Am. Meteorol. Soc. 79 (1), 61–78. https://doi.org/10.1175/1520-0477(1998)079<0061:APGTWA>2.0.CO;2.

Torrence, C., Webster, P.J., 1999. Interdecadal changes in the ENSO–monsoon system. J. Clim. 12 (8), 2679–2690. https://doi.org/10.1175/1520-0442(1999)012<2679:ICITEM>2.0.CO;2.

Troccoli, A., Dubus, L., Haupt, S.E., 2014. Weather Matters for Energy. Springer New York, New York, NY https://doi.org/10.1007/978-1-4614-9221-4.

von Bremen, L., 2010. Large-Scale Variability of Weather Dependent Renewable Energy Sources. Springer, Dordrecht, pp. 189–206. https://doi.org/10.1007/978-90-481-3692-6_13.

Weitemeyer, S., Kleinhans, D., Vogt, T., Agert, C., 2015. Integration of renewable energy sources in future power systems: the role of storage. Renew. Energy 75, 14–20. https://doi.org/10.1016/j.renene.2014.09.028.

Weitemeyer, S., Kleinhans, D., Wienholt, L., Vogt, T., Agert, C., 2016. A European perspective: potential of grid and storage for balancing renewable power systems. Energy Technology 4 (1), 114–122. https://doi.org/10.1002/ente.201500255.

Widen, J., 2011. Correlations between large-scale solar and wind power in a future scenario for Sweden. IEEE Transactions on Sustainable Energy 2 (2), 177–184. https://doi.org/10.1109/TSTE.2010.2101620.

Widén, J., Carpman, N., Castellucci, V., Lingfors, D., Olauson, J., Remouit, F., Bergkvist, M., Grabbe, M., Waters, R., 2015. Variability assessment and forecasting of renewables: a review for solar, wind, wave and tidal resources. Renew. Sust. Energ. Rev. 44, 356–375. https://doi.org/10.1016/j.rser.2014.12.019.

Wörman, A., Bottacin-Busolin, A., Zmijewski, N., Riml, J., 2017. Spectral decomposition of regulatory thresholds for climate-driven fluctuations in hydro- and wind power availability. Water Resour. Res. 53 (8), 7296–7315. https://doi.org/10.1002/2017WR020460.

Zaramella, M., Borga, M., Zoccatelli, D., Carturan, L., 2019. TOPMELT 1.0: a topography-based distribution function approach to snowmelt simulation for hydrological modelling at basin scale. Geosci. Model Dev. 12 (12), 5251–5265. https://doi.org/10.5194/gmd-12-5251-2019.

Zolezzi, G., Bellin, A., Bruno, M.C., Maiolini, B., Siviglia, A., 2009. Assessing hydrological alterations at multiple temporal scales: Adige River, Italy. Water Resour. Res. 45 (12). https://doi.org/10.1029/2008WR007266.